Macromolecules **2006,** *39,* 2191−2200

Heterogeneity of the Surfactant Layer in Organically Modified Silicates and Polymer/Layered Silicate Composites

G. Panek, S. Schleidt, Q. Mao, M. Wolkenhauer, H. W. Spiess, and G. Jeschke*

Max Planck Institute for Polymer Research, Postfach 3148, 55021 Mainz, Germany

Received December 23, 2005; Revised Manuscript Received February 2, 2006

ABSTRACT: Dynamics and microstructure of the surfactant layer in organically modified silicates and their composites with polystyrene were studied as a function of surfactant loading and temperature in the range relevant for melt intercalation. Site selectivity was achieved by using specifically headgroup- and tail-labeled surfactant EPR spin probes and by applying ^{31}P MAS NMR to phosphonium surfactants. Bimodal dynamics is observed over a broad range of surfactant loadings and temperatures in both the absence and presence of polymers and correlates with a bimodal distribution of surfactant headgroup distances from the silicate surface. Excess surfactant with respect to the cation exchange capacity of the silicate plasticizes the surfactant layer. Electron spin echo envelope modulation on nanocomposites with ammonium surfactant and deuterated polystyrene demonstrates close contact between the polymer and surfactant tail ends. Surfactant dynamics changes strongly during microcomposite formation, i.e., by embedding stacks of organoclay platelets in a polymer matrix, even if no intercalation takes place.

Introduction

Nanodispersed silica platelets can improve heat resistance,[1] storage and loss modulus, tensile strength, gas barrier, and flame-retardant properties of polymers without increasing brittleness or compromising transparency of the material.[2,3] For hydrophobic polymers, which are more commonly used as construction materials than hydrophilic polymers, nanodispersion usually presupposes that the layered silicates are compatibilized by amphiphiles. For instance, cationic surfactants such as alkylammonium and alkylphosphonium salts compatibilize the clay minerals hectorite and montmorillonite or synthetic layered silicates of similar composition. The resulting organoclays are the most commonly studied and applied nanofillers in polymers.[3]

Structural characterization of organoclays and their nanocomposites with polymers is mainly performed with wide-angle X-ray scattering (WAXS) and transmission electron microscopy (TEM), which provide information on morphology. Summary information on dynamic phenomena is obtained by dynamic mechanical analysis and melt rheology. While these established techniques are extremely useful for empirical materials development and application, they are of limited value for an understanding of the composites on a molecular level. Solid-state nuclear magnetic resonance (NMR)[4] has recently emerged as a technique that can provide more detailed information on polymer chain ordering,[5] and phase structure[6] as well as information on interaction of the polymer with silicate platelets[7] and on polymer dynamics.[8] Dynamics in the organic−inorganic interface of related nanocomposite gels have been addressed by a combination of NMR and spin-label electron paramagnetic resonance (EPR) spectroscopies.[9]

Although the importance of the composite interface is generally acknowledged,[10] none of the spectroscopic studies on nanocomposites have addressed the surfactant layer, which is crucial for nanodispersion of the silica platelets[11] and additionally influences mechanical properties by plasticizing the polymer.[12] The relation between surfactant structure and surfactant loading of the layered silicate on one hand and favorable interaction of the organoclay with the polymer and improvement of mechanical properties on the other hand is not yet understood on a fundamental level, although empirical rules could be derived by varying surfactant structures in melt intercalation[13] of organoclays by polystyrene.[14]

Following a preliminary report of our own,[15] and recent FTIR,[16] NMR,[17] and molecular dynamics (MD)[18] work of others on surfactants in organoclays, we now introduce a new approach for studying structure and dynamics of the surfactant layer. This approach is mainly based on EPR experiments on surfactant spin probes and uses complementary information from solid-state NMR on surfactant headgroups. In particular, we address heterogeneity of surfactant dynamics as a function of surfactant loading and temperature, differences in dynamics between the surfactant headgroups and tails, and changes in surfactant dynamics caused by formation of polymer composites. Using an electron spin echo envelope modulation (ESEEM) technique,[19] we further characterize contact between the polystyrene chain and the surfactant. We restrict ourselves to melt intercalation, which has become the standard method of preparation of polymer/layered silicate nanocomposites.[3] Besides the commonly used ammonium surfactants, we also consider a phosphonium surfactant because of its higher thermal stability[20] and better suitability for headgroup-selective NMR.

The paper is organized as follows. First, the morphology of the polymer−clay composites is considered on the basis of WAXS data. The temperature dependence of surfactant dynamics close to the headgroup and tail end is then elucidated on the basis of CW EPR data in pure organoclays and polymer−clay composites with different morphology. This section emphasizes different parameters for characterization of the spectral line shape and their complementary information content. Furthermore, solid-state NMR data are analyzed to characterize surfactant loading of the clays and to obtain further insight into temperature-dependent surfactant dynamics and structure of the surfactant layer. The Results section concludes with an analysis of ESEEM data of clay composites with deuterated PS that provide information on contacts between surfactant and polymer.

---

* Corresponding author: e-mail jeschke@mpip-mainz.mpg.de; Ph +49-6131-379 247; Fax +49-6131-379 100.

10.1021/ma0527449 CCC: $33.50

Chart 1. Structures of HTBP and of Surfactant Spin Probes

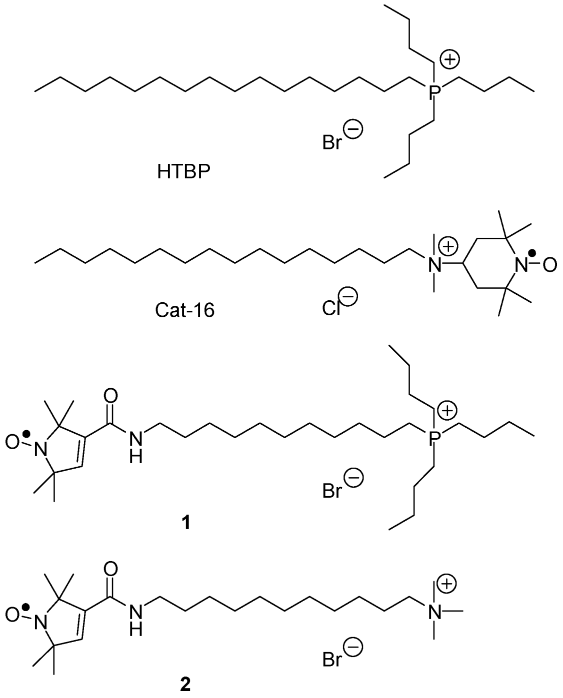

The following section discusses the picture of the surfactant layer in pure organoclays and polymer−clay composites that is suggested by this combination of different techniques.

Experimental Section

Materials. Synthetic fluoromica Somasif ME-100 was a gift from Co-Op Chemical Co., Japan. Tributylhexadecylphosphonium bromide (HTBP, Aldrich), hexadecyltrimethylammonium chloride (HTMA, Aldrich), the headgroup labeled spin probe 4-(*N*,*N*-dimethyl-*N*-hexadecyl)ammonium-2,2,6,6-tetramethylpiperidine-1-oxyl-iodide (Cat-16, Molecular Probes, Inc.), and 4-oxo-2,2,6,6-tetramethylpiperidine-1-oxyl (TEMPONE, Aldrich) were used as received. The tail-labeled spin probes **1** with a phosphonium headgroup and **2** with an ammonium headgroup were synthesized in our own laboratory as described below. Characterization by NMR and MS is decsribed in the Supporting Information. Polystyrenes with a narrow molecular weight distribution (GPC standards, PS10K ($M_w \sim 9500$, $M_w/M_n \sim 1.06$, $T_g = 370$ K), PS30K ($M_w \sim 32\,000$, $M_w/M_n \sim 1.03$, $T_g = 374$ K), and PS100K ($M_w \sim 94\,900$, $M_w/M_n \sim 1.06$, $T_g = 377$ K)) were obtained from Fluka. Anionically polymerized perdeuterated polystyrene (PS10K-d_8, $M_w \sim 10\,950$, $M_w/M_n \sim 1.04$) was obtained from Polymer Laboratories, Inc.

Synthesis of Tail-Labeled Spin Probes. *2-(11-Bromoundecyl)-isoindole-1,3-dione.* 11-Bromoundecanol (Fluka, 5.0 g) and potassium phthalimide (Fluka, 2.7 g) were reacted for 5 h in DMF (20 mL) at 80 °C. After cooling down, the reaction mixture was dissolved in 40 mL of chloroform and extracted two times with 70 mL of water. The water phases were extracted two times with 20 mL of chloroform. The combined organic phases were washed first with 20 mL of 0.2 M NaOH and then with 20 mL of water. The solution was dried (Na_2SO_4). The solvent was removed in vacuo, and 2-(11-hydroxyundecyl)isoindole-1,3-dione was obtained as a colorless solid (5.58 g, 88%). Tetrabromomethane (Fluka, 4.7 g), triphenylphosphine (Aldrich, 3.7 g), and 2-(11-hydroxyundecyl)-isoindole-1,3-dione (3.0 g) were stirred overnight in diethyl ether (60 mL) at room temperature. Filtration over silica gel with petroleum ether/aceton (5:1) as a solvent gave 2-(11-bromoundecyl)-isoindole-1,3-dione (1,72 g, 72%) as a pale yellow solid.

Quaternization. For compound **1**, to tributylphosphine (Fluka, 1.73 mL) at 90 °C a solution of 2-(11-bromoundecyl)isoindole-1,3-dione (2.8 g) in dry acetone (20 mL) was added under argon. After stirring for 20 h and evaporation of the solvent, tributyl-[11-(1,3-dioxo-1,3-dihydroisoindol-2-yl)undecyl]phosphonium bromide (**1a**) was obtained as a yellow oil after distillation in vacuo (3.68 g, 90%). For compound **2** to a solution of 2-(11-bromoundecyl)-isoindole-1,3-dione (1.53 g) in ethanol (55 mL) an aqueous solution of trimethylamine (Fluka, 45−50%, 8.2 mL) was added. After stirring for 7 days at room temperature and removing the solvent and excess of trimethylamine at 45 °C and a pressure of 110−120 mbar the yellow, solid residue was dissolved in ethanol (30 mL) and precipitated using diethyl ether (120 mL) to give trimethyl-[11-(1,3-dioxo-1,3-dihydroisoindol-2-yl)undecyl]ammonium bromide (**2a**) as a pale yellow solid (1.29 g, 75%).

Deprotection and Spin-Labeling. An aqueous solution of hydrazine hydrate (Fluka, 25%, 2.5 mL) and methanol (100 mL) and **1a** (2.51 mL) or **2a** (1.29 g) were refluxed for 1 h. After addition of water and evaporation of methanol, concentrated hydrochloric acid was added and the mixture was further refluxed for 1 h. After cooling down, a white precipitate was removed and the clear yellow solution was extracted two times with 30 mL of ethyl acetate. The aqueous phase was concentrated to dryness, and (11-aminoundecyl)-tributylphosphonium bromide (**1b**, yellow oil, 2.28 g, 80%) or (11-aminoundecyl)trimethylammonium bromide (**2b**, yellow solid, 0.53 g, 58%) was obtained. For spin-labeling, to a solution of **1b** (0.39 g) or **2b** (0.27 g) in dry THF (15 mL) were added 2,2,5,5-tetramethyl-3-pyrroline-1-oxyl-3-carboxylic acid (Aldrich, 0.24 g) and DMAP (Merck, 0.36 g). DCC (Fluka, 0.54 g) was added under ice cooling, and the mixture was then stirred for 3 days at room temperature. After separating from the precipitated urea to the clear yellow solution 2 M HCl (40 mL) was added. The mixture was extracted two times with 20 mL of diethyl ether, the combined organic phases were dried (Na_2SO_4), and the solvent was removed in vacuo. Compound **1** (orange crystalline solid, 1.59 g, 51%) and compound **2** (yellow solid, 0.38 g, 91%) were obtained. The identity of the compounds was checked by mass spectroscopy, ^{1}H NMR, and ^{13}C NMR and for paramagnetic substances by IR spectroscopy.

Preparation of Organoclay. To a dispersion prepared by stirring 2 g of Somasif ME-100 in 200 mL of deionized water for about 30 min was added a solution of the appropriate amount of HTBP and spin probes (if required) in a mixture of 40 mL of deionized water and 40 mL of ethanol that was kept at 60 °C. Surfactant-excess samples were prepared by using a 3-fold excess of HTBP with respect to the cation exchange capacity (CEC: 0.85 mequiv/g) of Somasif ME-100 while for surfactant-deficient samples the amount of HTBP was 0.8 times the CEC. For NMR experiments, samples with other ratios R_{th} of the amount of surfactant to the CEC were prepared as mentioned in the text, and the actual surfactant to CEC ratio R_{exp} was determined by quantitative solid-state NMR. Surfactant-excess samples with the ammonium surfactant HTMA were prepared analogously. The amount of spin probes used (Cat-16: 2 mg, **1**: 5 mg, **2**: 20 mg) ensured less than 2% of foreign surfactant molecules were introduced, and no spectral broadening due to dipole−dipole interaction between electron spins was observed. After stirring the combined solutions at 60 °C for 5 h, the precipitate was collected by filtration and washed with an 1:1 hot mixture of deionized water and ethanol until an $AgNO_3$ test for chloride ions in the washing liquid was negative. The obtained material was dried in the vacuum oven at 70 °C for 24 h. Unless stated otherwise, EPR and NMR samples were prepared by pressing 100 mg of organoclay at a temperature of 433 K for 30 min at 70 MPa in a Weber-Press (Maschinen Apparatebau GmbH).

Preparation of Nanocomposites. Mixtures of 75 mg of polymer and 25 mg of organoclay were pressed at temperatures of 433 K for 30 min at 70 MPa in a Weber-Press.

EPR Measurements. Spectra were recorded on a Bruker ELEXSYS 580 EPR spectrometer at X-band frequencies (9.3−9.8 GHz). Variable-temperature CW EPR was performed with a 4103 TM resonator using a glass dewar and the Bruker ER 4111 VT temperature control unit. A microwave power of 2 mW, modulation amplitude of 0.1 mT, and a modulation frequency of 100 kHz were employed. Three-pulse ESEEM experiments[19] were performed at a temperature of 50 K and at the maximum of the nitroxide spectrum using a a Bruker Flexline split-ring resonator ER 4118X_MS3. Pulse

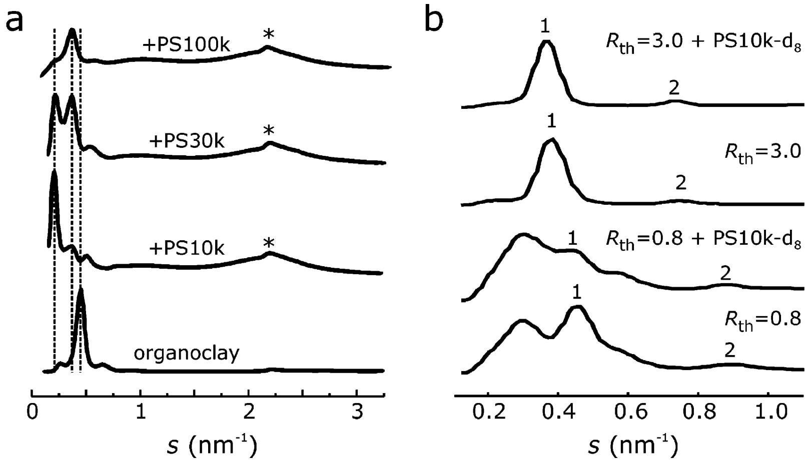

Figure 1. WAXS data for Somasif-based organoclays and their composites with polystyrene. (a) Surfactant-excess organoclay prepared with HTMA and its composites with PS10K, PS30K, and PS100K (from bottom to top). The asterisk denotes a peak from the crystalline domains of PS. Composite data have been normalized to this peak. Vertical dashed lines are guides for the eyes. (b) Organoclays prepared with HTBP and their composites. The peak assigned to d_{001} (1) and the peak at twice the corresponding s value (2) are labeled. Bottom to top: surfactant-deficient organoclay, its nanocomposite with PS10K-d_8, surfactant-excess organoclay, and its nanocomposite with PS10K-d_8.

widths were 16 ns, and the interpulse delay between the first two pulses was 344 ns to obtain a favorable ratio of deuterium to proton modulations. An increment of 16 ns was used for the second interpulse delay, and 512 data points were acquired.

NMR Measurements. Spectra were recorded on a Bruker ASX 500 spectrometer. Samples were placed in 4 mm rotors and spun at an MAS frequency of 12 kHz. Free-induction decay signals were recorded after a 90° pulse of 4.2 μs duration, and T_1 measurements were performed with an inversion recovery sequence. Ammonium dihydrogen phosphate (ADHP, Aldrich) was used as a ^{31}P chemical shift reference ($\delta = 0.8$ ppm)[21] and as an internal reference (20 wt %) for spin counting of surfactant headgroups. Variable-temperature MAS experiments were performed with nitrogen bearing gas for sample spinning to avoid oxidative decomposition.

Further Sample Characterization. All wide-angle X-ray scattering (WAXS) measurements were performed on a custom-made setup consisting of an X-ray generator and an X-ray mirror to parallelize the beam and therefore to minimize the beam divergence. Using a pinhole collimation system, the beam diameter is about 0.7 mm. A double graphite monochromator for Cu Kα radiation with a wavelength $\lambda = 0.154$ nm was used. For data acquisition a two-dimensional detector (Bruker AXS) with 1024 × 1024 pixels was utilized. The sample-to-detector distance was 80 mm; therefore, the accessible scattering angle range was $2° < 2\theta < 32°$. After background subtraction the scattered intensity distributions were integrated over the azimuthal angle and are presented as a function of the scattering vector $s = 2 \sin \theta/\lambda$. Basal spacings d_{001} of the layered silicate are thus given by Bragg's law by $1/s_{001}$, where s_{001} is the scattering vector corresponding to the first-order peak. DSC and TGA measurements were performed on Mettler DSC 30 and Mettler TG 851 systems.

Automated Data Analysis of CW EPR Spectra. The integrated spectrum and the double integral D of the spectrum were computed after linear baseline correction. The center field $B_{0,c}$ of the line shape was associated with the maximum of the integrated spectrum in the range of ±1.22 mT around the center of the field sweep.

Extrema Separation of the Slow Component. A fifth-order polynomial was fitted to the range between $B_{0,c} - 4.9$ mT and $B_{0,c} - 3.0$ mT, and an approximation $B^{(0)}{}_{0,\mathrm{lf}}$ of the low-field maximum was associated with the maximum of this polynomial. An improved value $B^{(1)}{}_{0,\mathrm{lf}}$ was obtained form a fifth-order polynomial fit in the range ($B^{(0)}{}_{0,\mathrm{lf}} - 0.6$ mT, $B^{(0)}{}_{0,\mathrm{lf}} + 0.6$ mT) and the final value $B_{0,\mathrm{lf}}$ by a fifth-order polynomial fit in the range ($B^{(1)}{}_{0,\mathrm{lf}} - 0.3$ mT, $B^{(1)}{}_{0,\mathrm{lf}} + 0.3$ mT). The high-field minimum $B_{0,\mathrm{hf}}$ was obtained analogously with a starting range ($B_{0,c} + 3.0$ mT, $B_{0,c} + 4.6$ mT). The extrema separation $2A'_{zz}$ for the slow component is given by $B_{0,\mathrm{hf}} - B_{0,\mathrm{lf}}$. This procedure corresponds to noise filtering with a filter adapted to the width of the spectral features at the extrema. It was tested against determination from the absolute high-field maximum and low-field minimum for noiseless simulated spectra, and the $2A'_{zz}$ values were found to coincide.

Width of the Central Line. The low-field maximum and high-field minimum for the central line were determined analogously to the corresponding extrema of the whole spectrum with starting intervals ($B_{0,c} - 0.6$ mT, $B_{0,c}$) for the maximum and ($B_{0,c}$, $B_{0,c} + 0.6$ mT) for the minimum. The fitting intervals were consecutively narrowed to 0.3 and 0.15 mT.

Extraction of the Fast Component. Automatic detection of the low field associated with the fast component was attempted by finding a minimum and maximum in the line shape in the range ($B_c - 1.555$ mT, $B_c + 1.495$ mT) that were distinct from the range limits. If both the minimum and maximum were found, starting values for fitting of a Voigt line were taken from the amplitude difference and field difference of these extrema. Voigt lines were used as the shape of the individual lines of a nitroxide three-line spectrum is a convolution of a Lorentzian (relaxational broadening) with a Gaussian (hyperfine couplings to protons). Voigt lines provide good fits for spectra that contain only a fast component. The sum of a Voigt line and a second-order polynomial background function was then fitted in the above-mentioned range. The Voigt line was associated with the low-field line of the fast component, simulated for the total range of the spectrum, and its double integral D_{lf} was computed. The high-field line and its double integral D_{hf} were obtained analogously in the range ($B_c + 1.495$ mT, $B_c + 1.555$ mT). In cases where only the high-field line could be detected, the fraction f_{fast} of the fast component was computed as $3D_{\mathrm{hf}}/D$; otherwise, it was computed as $1.5(D_{\mathrm{lf}} + D_{\mathrm{hf}})/D$. Unlike total simulation of the composite spectrum, this technique does not depend on having a suitable model for the motion of the probes. It is limited to cases with only two major components that differ in rotational correlation times by at least 1 order of magnitude. Matlab (The MatWorks, Inc.) programs implementing these data analysis are available from the authors on request.

Results

WAXS. Intercalation of polymer chains into the galleries of organoclays can be proved by observing the change in lamellar spacing by WAXS.[3] For organoclays prepared from the ammonium surfactant HTMA on Somasif ME-100, we have studied this change as a function of molecular weight of monodisperse PS intercalants (Figure 1a). The peak marked with an asterisk stems from the PS. Peaks corresponding to the basal spacing of silicate sheets are found in the range $s < 0.5$ nm^{-1}. For unmodified Somasif Me-100, a basal spacing of $d_{001} = 1.227$

nm has been reported.[22] In our own WAXS data (not shown) we find a peak that can be assigned to this spacing but also additional peaks that indicate superstructure or some heterogeneity of the material. The additional peaks vanish for surfactant loadings larger than the CEC, and only one well-defined peak in the range of the basal spacing is observed (bottom trace in Figure 1a).

For such surfactant-excess organoclays prepared with HTMA we find a basal spacing of $d_{001} = 2.16$ nm, which compares to literature values of 1.41−1.44 nm for monolayers (surfactant-deficient samples) and 1.77 nm for bilayers (surfactant-matched samples) of HTMA in organoclays based on the different clay mineral montmorrillonite, which has a similar CEC of 0.82 mequiv/g.[23] In fluorohectorites with a CEC of 1.5 mequiv/g, a basal spacing of ∼2.2 nm was found when using an excess of primary ammonium ions with one hexadecyl chain, which is very similar to our value.

Composite formation with PS10K in our case causes an increase of the basal spacing to $d_{001} = 3.38$ nm (second trace from bottom in Figure 1a). For a three time larger molecular weight of the polymer (PS30K), we also observe a very similar spacing $d_{001} = 3.26$ nm, but also a spacing of 2.21 nm, which is very close to the one in the organoclay before composite formation. With even higher molecular weight of the polymer (PS100K, top trace in Figure 1a), only a spacing of 2.20 nm is found, which is very close to the spacing before composite formation. These results indicate complete intercalation (nanocomposite formation) with PS10K, partial intercalation with PS30K (mixture of nanocomposite and microcomposite), and no significant intercalation (microcomposite formation) with PS100K. In further tests we have found that intercalation by PS with higher molecular weight can be improved by increasing temperature or duration of the thermal treatment (data not shown), but only at the expense of losing part of the spin probes by thermal decomposition. We therefore decided to restrict further studies to PS10K.

For surfactant-deficient ($R_{\mathrm{th}} = 0.8$) and surfactant-excess ($R_{\mathrm{th}} = 3.0$) organoclays prepared from Somasif ME-100 and HTBP, we found basal spacings of $d_{001} = 2.21$ and 2.65 nm, respectively. In both cases, the d_{002} peaks are clearly observed (see labels 2 in Figure 1b). Note that the actual surfactant excess in the samples with $R_{\mathrm{th}} = 3.0$ is only 70% over the CEC ($R_{\mathrm{exp}} = 1.7$) as found by quantitative NMR (see below). The basal spacings for HTBP compare to literature values of 1.87 nm in smectite (CEC 0.87 mequiv/g), 2.13 nm in montmorrillonite (CEC ∼ 1.1 mequiv/g), and 2.44 nm in modified mica (CEC ∼ 2.5 mequiv/g).[24] In Somasif ME100 with a larger size of the platelets and a lower CEC, we thus find a larger basal spacing, which supports the hypothesis of Maiti et al. that the basal spacing increases with size of the clay platelets but conflicts with their assumption that the CEC plays a more important role.[24] The considerable difference in the basal spacings between the two samples indicates the importance of controlling the actual amount of surfactant used in the preparation of the organoclay.

Much to our surprise, the basal spacings of HTBP organoclay change only slightly on formation of the composite with PS10K-d_8. For the surfactant-deficient organoclay we find a change from 2.21 to 2.28 (two lowermost traces in Figure 1b) and for the surfactant-excess organoclay a change from 2.65 to 2.72 nm (two uppermost traces in Figure 1b). Although these changes are reproducible, they are very close to the resolution limit to the detector and do not allow for firm conclusions about structural changes. In the case of surfactant-deficient organoclay the shapes of the scattering curves before and after composite formation are somewhat different, so that partial intercalation cannot be completely ruled out. However, for surfactant-excess HTBP organoclay only a small shift in d_{001} is observed, which is not consistent with significant intercalation. Instead, it is likely that the HTBP layer in a microcomposite cannot reach its thermal equilibrium structure during cooling of the material since the PS matrix, in which the stacks of clay platelets are embedded, solidifies at a temperature that is higher than the order−disorder transition of the HTBP layer.

The failure of intercalation of PS10K into surfactant-excess HTBP organoclay was reproduced with both protonated and deuterated PS and with several samples of independently prepared organoclay. Likewise, successful intercalation of PS10K into HTMA organoclay was reproduced with both protonated and deuterated PS and with independently prepared organoclay samples. Hence, the same combination of polymer (PS10K) and clay (Somasif ME-100) reproducibly forms microcomposites when the phosphonium surfactant HTBP is used and nanocomposites when the ammonium surfactant HTMA is used. This provides a unique opportunity for testing whether changes in structure and dynamics of the surfactant layer during composite formation do or do not depend on intercalation.

CW EPR Spectroscopy. EPR spectroscopy of unmodified Somasif ME-100 at W-band frequencies (9.6 GHz) reveals a broad and relatively weak spectrum with a maximum near $g = 2$ that we ascribe to an Fe(III) impurity (data not shown). At W-band frequencies (94.2 GHz) this contribution dominates the CW EPR spectrum even for spin-labeled organoclays (see Supporting Information). For organoclays at X-band frequencies, transverse relaxation times of the nitroxides at 50 K are unusually low (200−300 ns instead of more than a microsecond). However, the Fe(III) contribution is almost negligible compared to the nitroxide in CW EPR, and it is not directly observed in pulsed EPR.

In previous work we have found surfactant fractions with different mobility in organoclays prepared with an excess of the ammonium surfactant HTMA.[15] For organoclays and microcomposites containing Somasif ME-100 as the silicate component and an excess of the phosphonium surfactant HTBP, this dynamical heterogeneity is even more pronounced, and the spectra can be described quite nicely in terms of two surfactant fractions, as is demonstrated in Figure 2a,b for the tail-labeled spin probes **1** and **2**. The fast fraction (circles) corresponds to rotational correlation times well below 3 ns and the slow fraction (squares) to rotational correlation times above 3 ns. To understand the origin of this heterogeneity of surfactant dynamics, we studied the dependence of the fraction of fast surfactant molecules on temperature and on composition of the material. This fraction can be quantified by fitting the narrow low-field and high-field lines (see dotted lines in bottom trace of Figure 2a) and relating their intensity (double integral) to the double integral of the whole spectrum (see Materials and Methods). For both head-labeled and tail-labeled spin probes and in both the absence and presence of polymer, we find a gradual increase of the fast fraction with temperature (see Figure 3). Heterogeneity of surfactant dynamics persists up to the highest temperatures at which the spin probes are stable (433−463 K, depending on the material as explained below).

Because of the large and variable fast fraction and the large aspect ratio of the Somasif silicate platelets (lateral dimension ∼1 μm, thickness 1 nm), we can exclude an assignment of the fast component to the edges of the platelets. Some insight into

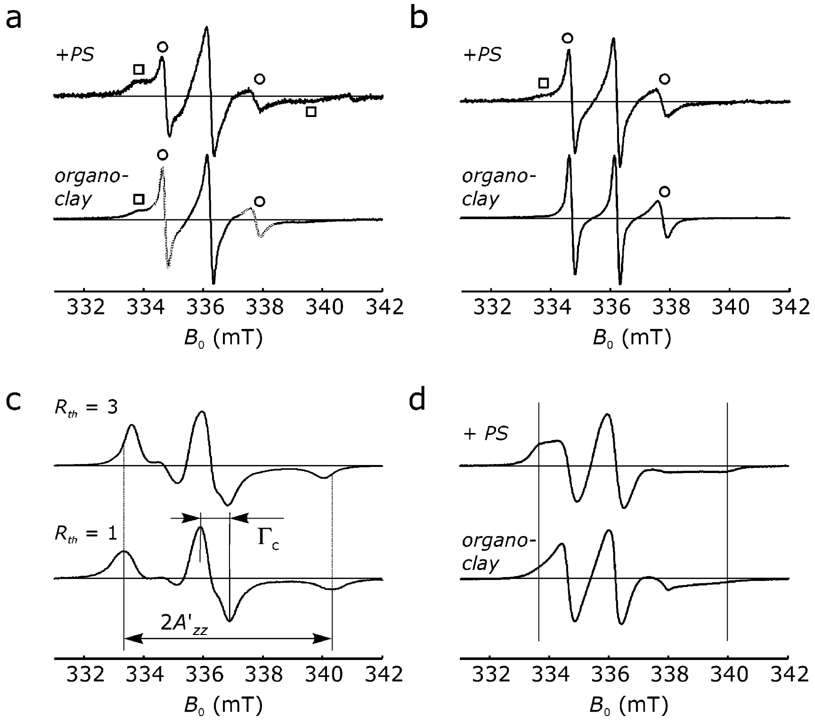

Figure 2. Representative CW EPR spectra of spin-labeled surfactants in organoclays (HTBP on Somasif ME-100) and their polymer composites. Narrow lines are guides to the eyes. (a) Tail-labeled phosphonium surfactant **1** in a surfactant-excess organoclay in the absence of polymer (bottom) and after microcomposite formation with PS10K (top) at 373 K. The dotted lines in the bottom trace are fits of the fast component. (b) Tail-labeled ammonium surfactant **2** in a surfactant-excess organoclay in the absence of polymer (bottom) and after microcomposite formation with PS10K (top) at 373 K. (c) Cat-16 in a surfactant-deficient (bottom) and surfactant-excess (top) organoclay at $T = 293$ K. (d) Cat-16 in a surfactant-excess organoclay in the absence of polymer (bottom) and after composite formation with PS10K (top) at $T = 373$ K.

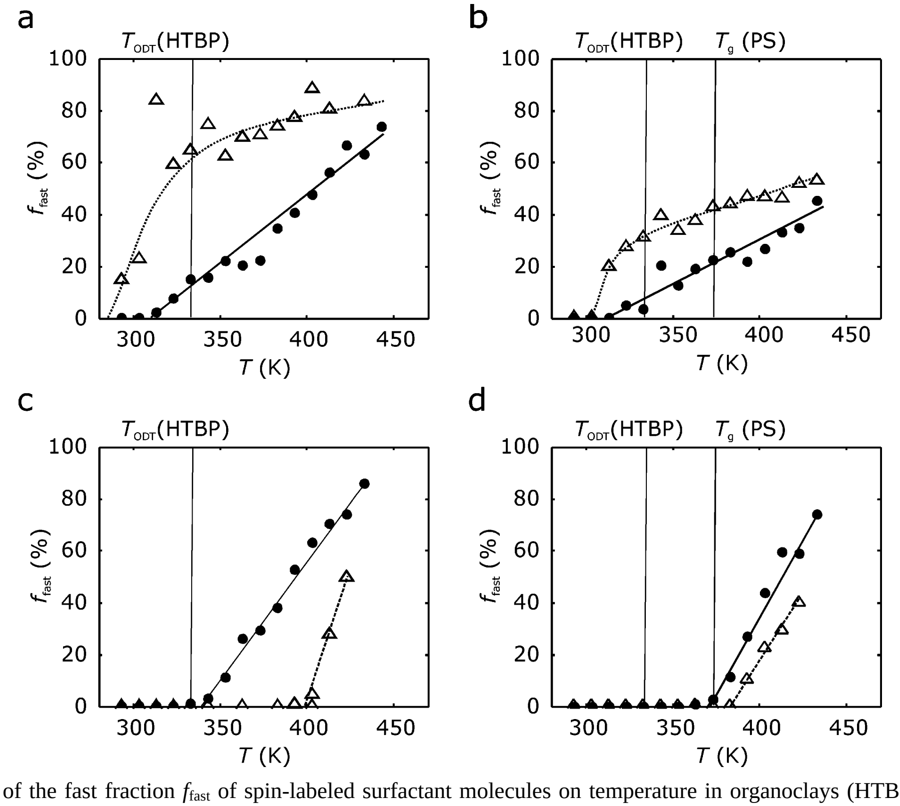

Figure 3. Dependence of the fast fraction f_{fast} of spin-labeled surfactant molecules on temperature in organoclays (HTBP on Somasif) and their composites according to analysis of CW EPR spectra. Solid lines are guides to the eyes. (a) Tail-labeled phosphonium surfactant **1** (circles) and ammonium surfactant **2** (triangles) in surfactant-excess organoclay. (b) Tail-labeled phosphonium surfactant **1** (circles) and ammonium surfactant **2** (triangles) in microcomposites of surfactant-excess organoclay with PS10K. (c) Cat-16 in surfactant-deficient (triangles) and surfactant-excess (circles) organoclay. (d) Cat-16 in composites of surfactant-deficient organoclay (triangles) and surfactant-excess (circles) with PS10K.

the origin of the heterogeneity is obtained by varying surfactant coverage of the platelets, which can be quantified by the ratio R of surfactant loading to the CEC of the clay. The room temperature CW EPR spectrum of the head-labeled probe Cat-16 in a surfactant-deficient sample ($R = 0.8$) exhibits a larger extrema separation $2A'_{zz}$ than a surfactant-excess sample pre-

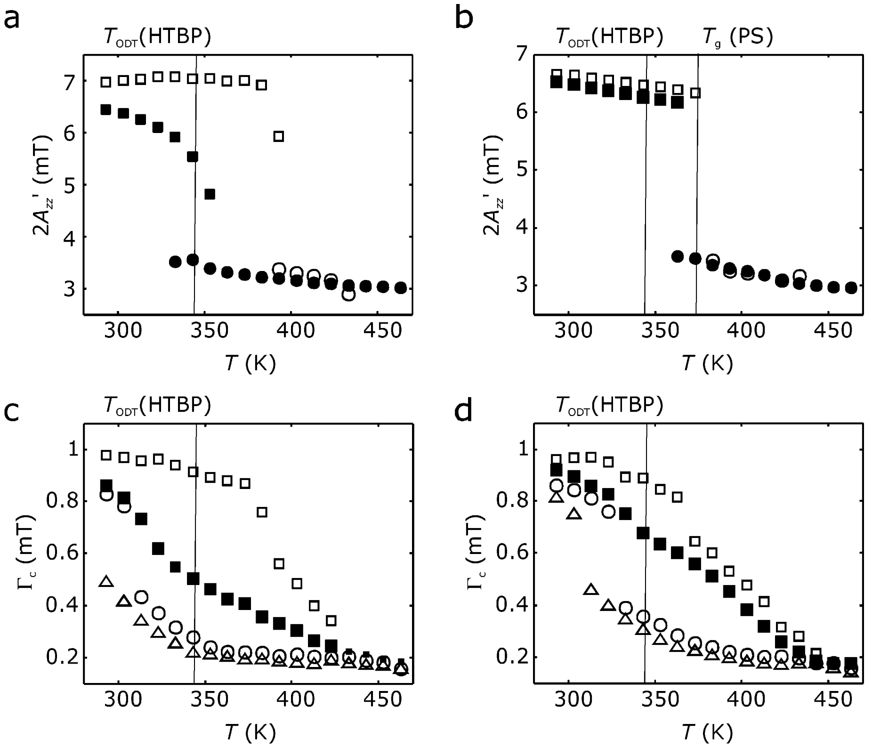

Figure 4. Dependence of extrema separations $2A'_{zz}$ and widths Γ_c of the central line in CW EPR spectra of surfactant spin probes in organoclays (HTBP on Somasif) and their composites with PS10K on temperature. (a) Extrema separations $2A'_{zz}$ for Cat-16 in surfactant-deficient (open symbols) and surfactant-excess (filled symbols) organoclay. Squares and circles correspond to the slow and fast component, respectively. (b) Extrema separations $2A'_{zz}$ for Cat-16 in polymer composites of organoclays. Open symbols correspond to surfactant-deficient and filled black symbols to surfactant-excess organoclay. Squares and circles correspond to the slow and fast component, respectively. (c) Line widths Γ_c for organoclays: open squares, Cat-16 in surfactant-deficient organoclay; filled squares, Cat-16 in surfactant-excess organoclay; open circles, tail-labeled phosphonium surfactant **1** in surfactant-excess organoclay; open triangles, tail-labeled ammonium surfactant **2** in surfactant-excess organoclay. (d) Line widths Γ_c for composites. Symbols as in (c).

pared with a 3-fold excess of HTBP with respect to the CEC (Figure 2c, the surfactant excess in the final material is only 1.7 as explained below). As $2A'_{zz}$ is reduced by rotational dynamics of the spin probe, this points to an increase of surfactant mobility with increasing surfactant coverage. As A_{zz} also depends on polarity of the environment of the spin probe,[25] this difference could also be due to on average higher polarity for the surfactant-deficient sample. However, quantitative analysis of the fast fraction (Figure 3c) suggests that, in the case at hand, increasing mobility with increasing surfactant coverage is the main contribution. In the surfactant-excess sample, surfactant molecules with rotational correlation times of their headgroups shorter than 3 ns are found at temperatures above 350 K, while in the surfactant-deficient sample no such surfactant headgroups are observed below 400 K. Note however that above 400 K two fractions can be clearly observed also in the surfactant-deficient sample, where all surfactant headgroups are supposed to be attached to negative charges on the silica surface.

According to DSC, the HTBP surfactant layer has a melting-like order−disorder transition between ~330 and ~350 K (T_{ODT} = 343 K), which is ~10 K above the melting point of the pure surfactant. Such behavior was previously observed for Cloisite organoclays, where T_{ODT} was found to be lower than the melting point of the pure surfactant.[26] In our case, tiny differences between the DSC curves of surfactant-deficient and surfactant-excess samples are observable but are hard to quantify and hard to reproduce. Interestingly, the decomposition temperature of headgroup-labeled Cat-16 gradually decreases when decreasing R from ~450 K at $R > 1$ to ~410 K at $R = 0.2$. This suggests that catalytic decomposition of the spin probe, and probably also of surfactant molecules, takes place at the clay surface.

Formation of the polymer microcomposite generally leads to a decrease of the fast fraction (Figure 2a,b) or at least to an increase of the average extrema separation $2A'_{zz}$ in the spectra that is to large to be explained by polarity changes. We may thus conclude that composite formation with PS immobilizes the surfactant layer significantly even if no intercalation takes place. In fact, such an effect can be expected for PS, whose glass transition temperature (T_g = 370 K) is higher than the order−disorder transition of the surfactant layer (T_{ODT} = 343 K). Below T_g the stacks of clay platelets embedded in the PS matrix cannot expand. In agreement with this consideration, the order−disorder transition of the surfactant layer is no longer observable in the DSC of the composites. With respect to the polymer, the DSC of microcomposites of PS10K with surfactant-deficient and surfactant-excess organoclay shows only a very slight decrease of T_g to 369 and 367 K, respectively.

Somewhat surprisingly, the change in surfactant dynamics by microcomposite formation cannot only be observed for the label at the tail end (compare Figure 3a,b) but also for the label at the headgroup (compare Figure 3c,d). However, in the latter case the effect is much more pronounced in surfactant-excess samples (circles), where at least some headgroups cannot be electrostatically attached to the clay surface, than in surfactant-deficient samples (triangles). Indeed, analysis of the central line width Γ_c indicates that headgroups in surfactant-deficient organoclays are slightly mobilized rather than immobilized on microcomposite formation with PS (see open squares in Figure 4c,d).

In a surfactant layer composed of a large excess of the phosphonium surfactant HTBP and a small fraction of tail-labeled ammonium surfactant **2**, we find higher mobility than in the analogous system with the tail-labeled phosphonium surfactant **1** (Figure 3a). As the majority surfactant is the same in both cases, and only the small amount of probe molecules has a different headgroup, dynamics of the layer should be the same. The result thus indicates that, in a mixed layer with an excess of phosphonium surfactant, ammonium surfactant molecules have a tendency to disengage from the silicate surface.

Alternatively, CW EPR spectra of spin-labeled surfactants can be quantified by determination of the extrema separations $2A'_{zz}$ for the fast and slow component (Figure 4). In particular, the values for the slow component may provide information that is complementary to the information obtained from quantifying the fast fraction. For instance, we find that $2A'_{zz}$ for the slow component in surfactant-excess samples (filled squares in Figure 4a) significantly decreases well before the fast component can be observed, while this is clearly not the case in the surfactant-deficient sample. The surfactant layer in the surfactant-deficient sample does not melt homogeneously, but much less heterogeneously than in the surfactant-excess sample. With a surfactant excess the layer melts more heterogeneously in the pure organoclay than in the microcomposite with PS10K (filled black squares in Figure 4a,b).

The average mobility of the whole surfactant population is most easily characterized by the width Γ_c of the central line (for definition, see Figure 2c), which is a parameter that can be determined with good precision by polynomial fitting even in spectra with rather poor signal-to-noise ratio. Furthermore, the parameter is highly sensitive to changes in dynamics over a broader range of rotational correlation times than $2A'_{zz}$ and combines information on the fast fraction and the mobility of the slow fraction. As Γ_c depends on g anisotropy and g_x depends on polarity of the spin probe environment,[25] this parameter is affected by changes in polarity and mobility, as is also the case for $2A'_{zz}$. For Cat-16 in surfactant-deficient organoclay, Γ_c detects a gradual increase in mobility already in the range between room temperature and 373 K, where $2A'_{zz}$ does not change significantly and no fast fraction is observable (open squares in Figure 4c). Up to temperatures of 433 K, headgroup mobility is higher in surfactant-excess (filled squares) compared to surfactant-deficient (open squares) organoclay. Rotational correlation times of surfactant tails (open triangles and circles) in surfactant-excess organoclays match the EPR time scale (nanoseconds) at temperatures that are ~60 K lower than for the headgroups. Up to 413 K surfactant tails of ammonium surfactants (open circles) move significantly faster than those of phosphonium surfacants (open triangles) when immersed in a layer that contains a large excess of phosphonium surfactants.

Comparison of Γ_c plots for organoclays and PS nanocomposites (Figure 4c,d) clearly reveals that microcomposite formation decreases the differences in surfactant dynamics, both between surfactant-deficient and surfactant-excess samples and between headgroup- and tailgroup-labeled surfactants. Dynamics of the whole surfactant layer appears to be dominated by dynamics of the matrix in which the stacks of clay platelets are embedded. On the other hand, all trends observed in the organoclays are still significant in the composites: surfactants are less mobile in surfactant-deficient organoclays than in surfactant-excess ones, tail ends are more mobile than headgroups, and ammonium surfactant headgroups are more mobile than phosphonium surfactant headgroups.

Solid-State NMR Spectroscopy. Nitroxide EPR spectra are more sensitive to small differences in dynamics than solid-state MAS NMR spectra and line shape analysis in terms of dynamics is more straightforward. However, MAS NMR can nicely complement the EPR results, as it does not require labeling of the surfactants and allows for a more precise quantification of the total amount of surfactant in an organoclay. To selectively address surfactant headgroups in complex materials, we use ^{31}P NMR with its comparatively high sensitivity (100% natural abundance, gyromagnetic ratio larger than for ^{13}C or ^{15}N) and absence of signals due to any other component of the system. To quantify spectral components, we employ experiments based on thermal polarization rather than cross-polarization from protons, despite the somewhat lower sensitivity associated with this approach. The total amount of surfactant is determined by admixture of a defined amount of ADHP and integration of the HTBP and ADHP peaks in the spectrum.

Using this technique, we have determined the composition of organoclays prepared with ratios R_{th} of the amount of surfactant to the CEC between 0.2 and 3.0 in increments of 0.2 (Figure 5a). Up to surfactant loadings of $R_{th} = 1.4$, we find agreement between the relative amount R_{th} of surfactant employed in the preparation and the amount R_{exp} found in the organoclay. In this range, the NMR spectra vary strongly with R_{th}. For higher R_{th}, the change in R_{exp} levels off and reaches a limiting value of ~1.7. In agreement with this observation, spectral line shapes do not change significantly between $R_{th} =$ 1.8 and 3.0.

Interestingly, the room temperature MAS NMR spectra contain a single broad peak at $\delta(^{31}\text{P}) \approx 31$ ppm for $R_{th} \leq 1$, while a second, narrower peak at $\delta(^{31}\text{P}) = 32.6$ ppm appears for $R_{th} > 1$ and increases in relative intensity with increasing R_{th} up to 1.8. It is natural to associate the former component with more immobile surfactant molecules, whose headgroups are directly attached to the silicate surface, and the latter component with more mobile molecules, whose headgroups are remote from the surface. The shift difference would then stem either from susceptibility differences, or from a contact shift due to a small amount of paramagnetic impurities (Fe^{3+}) in Somasif, or from slight changes in the electronic structure of the headgroup caused by electrostatic attachment. The assignment is supported by the temperature dependence of the ^{31}P MAS NMR spectra of a surfactant-deficient organoclay ($R_{th} =$ 0.8, Figure 5c) and a surfactant-excess organoclay ($R_{th} = 3.0$, Figure 5d). The spectra show a gradual increase of the relative intensity and of the chemical shift of the narrow peak. Similar observations have been made for $R_{th} = 0.6$ (data not shown). We have also checked by an inversion recovery measurement whether such a simple two-state model of attached and detached surfactant molecules is consistent. Somewhat to our surprise both NMR peaks exhibit monoexponential longitudinal relaxation at room temperature (Figure 5b) with relaxation times $T_{1,\text{mobile}} = 0.82$ s for the more mobile and $T_{1,\text{mobile}} = 2.15$ s for the more immobile fraction.

Closer analysis reveals, however, that the amount of immobilized surfactant molecules is not simply determined by the CEC, but rather depends on surfactant loading and temperature. For instance, for the highest loading $R_{exp} = 1.7$, the immobile fraction might be expected to amount to almost 60%, while only 30% of the intensity corresponds to the broad peak at 31 ppm. Furthermore, even in samples with surfactant coverages below the CEC, the narrow peak associated with mobile headgroups is observed at temperatures of 340 K and above (Figure 5c). Note that the CEC quantifies the number of negative surface charges that binds cations in solution at ambient temperature. It appears feasible that in a molten surfactant layer at higher temperature the number of contact ion pairs is lower than that.

Finally, the ^{31}P chemical shift at room temperature for the immobile fraction also slightly depends on surfactant coverage.

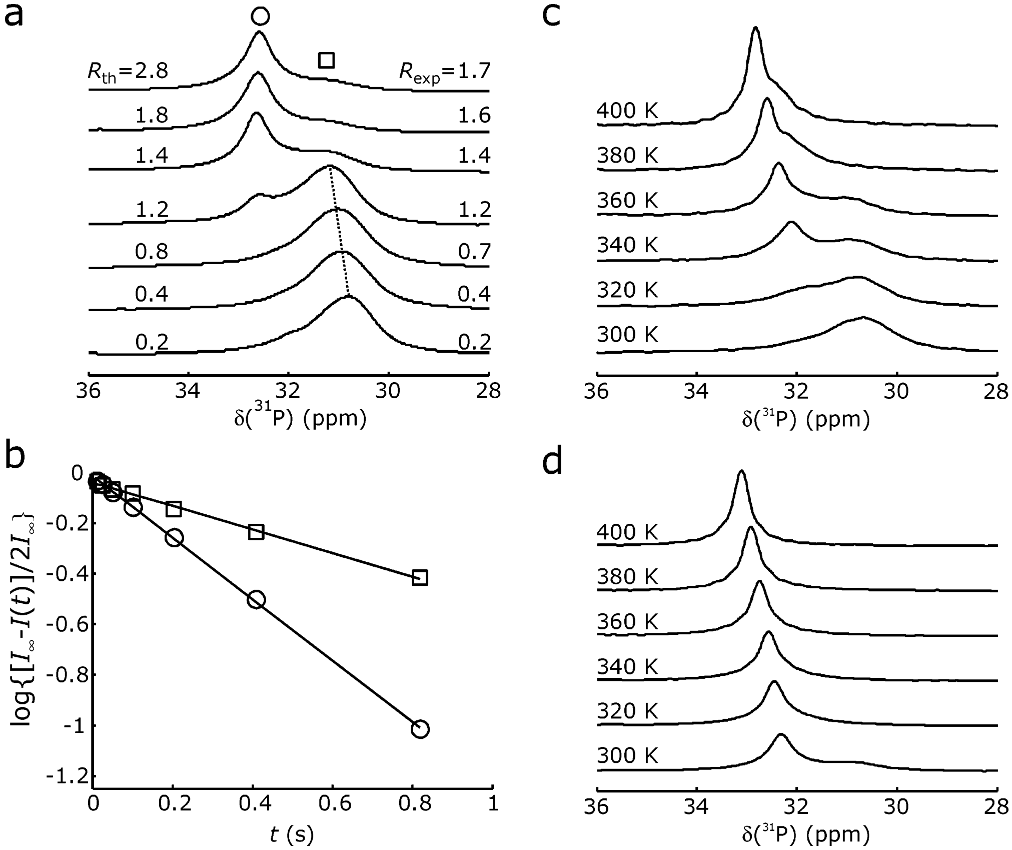

Figure 5. ^{31}P solid-state NMR on organoclays (HTBP on Somasif). (a) Dependence of the NMR spectrum on surfactant coverage. The circle and square designate the peaks of the more mobile and more immobile fraction, respectively. (b) Semilogarithmic plot of the nonequilibrium magnetization (arbitrary units) vs interpulse delay in an inversion recovery experiment for the peaks of the more mobile (circles) and more immobile (squares) surfactant fraction. The solid lines are linear fits. (c) Dependence of the NMR spectra on temperature for a surfactant-deficient sample (R_{th} = 0.8). (d) Dependence of the NMR spectra on temperature for a surfactant-deficient sample (R_{th} = 3.0).

It increases from 30.8 ppm at R_{th} = 0.2 to 31.2 ppm at R_{th} = 1.2 (see dotted line in Figure 5). These observations of gradual changes in mobility or in the interaction with the surface charges over large intervals of surfactant loading and temperature are similar to the observations made by EPR. Likewise, the occurrence of a fast fraction and a slow fraction of surfactant molecules with relative amounts depending on temperature is seen in both NMR and EPR spectra.

ESEEM Spectroscopy of Nanocomposites. As surfactant dynamics is strongly influenced by microcomposite formation, it cannot be used for detecting and characterizing the formation of nanocomposites by polymer intercalation. Intercalation is associated with spatial proximity of the polymer chains to the surfactant molecules and can thus be proved and characterized by measuring an interaction between the electron spin of a spin-labeled surfactant and a nuclear spin in the polymer chain. To introduce unambiguous contrast between polymer and surfactant, we use perdeuterated PS (PS-d_8) and observe deuterium ESEEM. At sufficiently long distances r > 0.25 nm the modulation depth in deuterium ESEEM scales with r^{-6} and with the average number of nuclei n that are at the distance of closest approach to the electron spin.[19] The decay rate of the modulation depends only on r^{-6}, but not on the number of nuclei, so that both parameters can be separated by data fitting (see below).

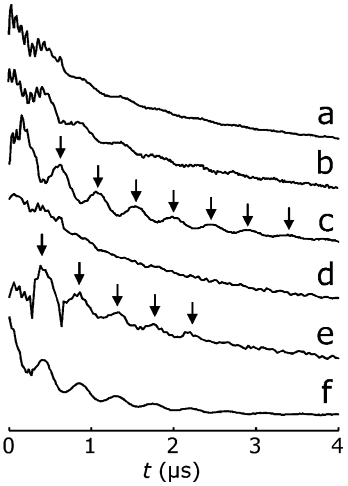

Figure 6. Three-pulse ESEEM on composites of organoclays (based on Somasif) with deuterated polystyrene PS10K-d_8. The arrows mark maxima of the deuterium modulation. (a) Surfactant-excess HTBP organoclay−PS microcomposite with head-labeled spin probe Cat-16. (b) Surfactant-deficient HTBP organoclay−PS composite with head-labeled spin probe Cat-16. (c) Surfactant-excess HTMA organoclay−PS nanocomposite with head-labeled spin probe Cat-16. (d) Surfactant-excess HTBP organoclay−PS microcomposite with tail-labeled spin probe **1**. (e) Surfactant-excess HTMA organoclay−PS nanocomposite with tail-labeled spin probe **2**. (f) TEMPON in pure PS10K-d_8.

In agreement with expectations from the WAXS results, strong deuterium modulations are observed with organoclays based on the ammonium surfactant HTMA (Figure 6c,e), while only weak (Figure 6a,b) or no modulations (Figure 6d) are observed with organoclays based on the phosphonium surfactant HTBP. The situation is most clear-cut for the tail-labeled surfactants **1** and **2** whose headgroups match the headgroups of the majority surfactant (Figure 6d,e). For **2** and Cat-16 in HTMA, the modulation depth is comparable to the one observed for TEMPONE in pure PS-d_8. This suggests intimate contact of the intercalated polymer and the surfactant. If the headgroup-labeled ammonium surfactant probe Cat-16 is incorporated into HTBP organoclay microcomposites with PS, weak deuterium modulation is observed. This is unexpected at least for the surfactant-excess sample (Figure 6a), which definitely does not exhibit significant intercalation. As already remarked for characterization of surfactant dynamics by CW EPR, this suggests that matching the headgroup of the surfactant spin probe to the headgroup of the majority surfactant is important for obtaining data that are representative for the whole layer. Otherwise, the distribution of the spin probe in the material may be different from the distribution of the majority surfactant. The somewhat stronger modulation for Cat-16 in the surfactant-deficient HTBP clay composite would be consistent with partial intercalation.

More quantitative information can be obtained by ratio analysis of the ESEEM data.[19,27] We consistently find a distance of closest approach of deuterium nuclei to the spin-label of 0.35−0.37 nm. This distance matches the expectation for van der Waals contact between the polymer chain and the nitroxide group of the spin-label. The average number of nuclei at that distance is $n \approx 0.25$ for the tail-labeled surfactant **2**, $n \approx 0.5$ for head-labeled Cat-16 in HTMA nanocomposite, and $n \approx 0.6$ for TEMPONE in pure PS-d_8. For Cat-16 in the HTBP microcomposites we find $n \approx 0.1$ with surfactant-excess and $n \approx 0.18$ with surfactant-deficient organoclay. An average number $n < 1$ means that only for a fraction of the spin probes a polymer chain is in van der Waals contact.

Discussion

Surfactant Layer in Organoclays. Both EPR and NMR spectroscopy demonstrate dynamical heterogeneity of the surfactant layer for surfactant loadings below and above the CEC. The fractions of the fast and slow components with surfactant loading and temperature make it rather unlikely that the bimodal behavior is solely due to heterogeneity of the silicate particle surface (patches). Wang et al. have observed similar bimodal behavior by ^{13}C NMR on an organoclay consisting of alkylammonium surfactants and montmorillonite, where they assigned peaks at $\delta(^{13}\mathrm{C}) = 33$ and 30 ppm to methylene groups in a more immobile ordered (all-trans) and a more mobile disordered (gauche and all-trans) microphase.[17] The shift difference was explained with a γ-gauche effect.[28] As in our experiments a gradual order−disorder transition was found. If we assume for the moment that the ^{31}P chemical shift dispersion is also dominated by a γ-gauche effect and that this effect is diamagnetic for ^{31}P as it is for ^{13}C, the different sign of the chemical shift difference in our case ($\delta(^{31}\mathrm{P}) \sim 33$ ppm for the mobile fraction and ∼31 ppm for the immobile fraction) would imply a trans conformation between P and C_γ for the mobile phase and a gauche conformation for the immobile phase. However, the marked temperature dependence of the chemical shift of both peaks (Figure 5c) rather suggests that paramagnetic shifts due to Fe^{3+} impurities in Somasif play a role. For high-spin Fe^{3+} ($S = {}^5/_2$) the pseudo-contact shift is proportional to $-D/(r^3T^2)$, where D is the (positive) zero-field splitting parameter and r is the distance of the ^{31}P nucleus to the Fe^{3+} ion.[29] The peak at ∼31 ppm would then correspond to headgroups that are closer to the surface of the silicate particle and the peak at ∼33 ppm to headgroups that are more remote. This interpretation is consistent with the larger width of the former peak which is then explained by expected variations in r, D, and the orientation of the P−Fe vector with respect to the zero-field tensor of the Fe^{3+} ion.

Interestingly, such a bimodal distribution of distances of surfactant headgroups normal to the surface of the silicate particle was suggested by recent MD simulations of quaternary alkylammonium surfactants on idealized montmorillonites ($R_{\mathrm{th}} = 1$).[30] The effect was particularly strong for HTMA, which is of the same type as HTBP (one hexadecyl chain). In these simulations, the majority fraction of surfactant molecules corresponds to the closer distance, as we find experimentally at ambient temperature. In the framework of earlier MD simulations for alkylammonium surfactants[18] and in the framework of the structural model of organoclays predicted on the basis of lamellar spacings,[22] the fraction of remote surfactant molecules would correspond to a partially occupied third layer. Such a picture is also consistent with the observed dependence of the EPR and NMR spectra on surfactant loading and temperature. For energetic reasons, sites closer to the surface are preferentially populated at small loadings and lower temperatures. The more remote sites have to be populated at $R_{\mathrm{th}} > 1$, but for entropic reasons they may also be populated at higher temperatures at $R_{\mathrm{th}} < 1$. Because of weaker electrostatic attachment, molecules at remote sites are more mobile.

EPR experiments on the tail-labeled surfactants demonstrate that the differences in mobility propagate to the surfactant tail ends. On the other hand, the fast fraction of tail ends does not exactly correspond to the fast fraction of headgroups. The fast fraction is generally larger for tail ends and exhibits an even more gradual increase with temperature. This suggests that the dynamics of a surfactant tail end is determined more strongly by collective behavior of neighboring surfactant molecules than by the degree of electrostatic attachment of the headgroup of the given molecule. Such collective effects would also explain the plasticizing effect on the surfactant layer that is observed with increasing surfactant coverage. In particular, excess surfactant may form patches of trilayer structures that are more mobile than the bilayer structures corresponding to $R_{\mathrm{th}} = 1$. Alternatively, bilayers and trilayers might alternate in the stacks of clay platelets. Foreign surfactants, as the tail-labeled ammonium surfactant **2** in a HTBP layer, appear to insert preferentially into such more mobile patches or layers. In general, the spectroscopic results suggest a much more complex picture than the melting-like order−disorder transition inferred from DSC.

Influence of Composite Formation on the Surfactant Layer. The dynamics of the surfactant layer is strongly changed already by embedding of stacks of organoclay platelets into the polymer, i.e., by microcomposite formation. Intercalation thus cannot simply be inferred from changes in surfactant mobility. Microcomposite formation generally moderates heterogeneity of surfactant dynamics (Figure 4c,d). In particular, the plasticizing effect of excess surfactant on the surfactant layer is much diminished. In stacks of surfactant-deficient organoclay platelets polymer embedding plasticizes the surfactant layer. This effect may be related to partial intercalation, which is suggested but not fully proved by our WAXS and ESEEM data. In surfactant-excess samples, the onset of formation of a fast fraction of surfactant headgroups on the EPR time scale (Figure 4c,d) shifts from the temperature of the melting-like order−disorder transition (343 K) to the glass transition temperature of PS (373 K).

For HTMA organoclay, the WAXS results imply intercalation of PS chains into the clay galleries and ESEEM data prove close contact between the chains and surfactant headgroups as well as tail ends. Note that modeling studies based on self-consistent-field techniques predict negligible interdigitation of surfactants with relatively short alkyl chains and long polymer chains.[31] This is somewhat at odds with our observation of van der Waals contact between the polymer and a label attached to the surfactant headgroup. Our experimental results may thus indicate that such a description with a single Flory−Huggins interaction parameter χ that considers only polymer−surfactant interactions may be oversimplified. The actual microstructure is expected to be a result of a simultaneous optimization of surfactant/silicate and surfactant/polymer contacts as well as the entropy of surfactant and polymer chains. Together with the observation that too closely matched structures of surfactant and polymer may actually prevent intercalation,[31] this indicates that the surfactant supports intercalation by moderating surface polarity rather than minimizing it. In other words, polar interactions of the polymer with the organically modified silica platelets may be crucial for optimizing the interaction energy, as was suggested in a recent review on the basis of empirical data.[3] The same reasoning was applied to explain the observation that nanocomposites obtained by melt-mixing nylon-6 with organoclays had better materials properties when using an equivalent amount of surfactant than when using excess surfactant.[32] This line of thought is consistent with partial intercalation of PS into surfactant-deficient HTBP organoclay and no significant intercalation into surfactant-excess organoclay, as indicated by the WAXS and ESEEM results. However, with respect to this we consider our present data as only weak evidence. Work with a different layered silicate and different polymers is planned to further investigate this point. In general, quantification of polymer−surfactant contacts by ESEEM may be useful for finding the surfactant loading that optimizes polar contacts between the organoclay and the polymer.

Conclusions

CW EPR spectroscopy on specifically spin-labeled surfactants can provide a detailed picture of dynamics of the surfactant layer in organically modified silicates and polymer/layered silicate composites. NMR and ESEEM measurements aimed at surfactant headgroups and tail ends supply complementary information on the structure of that layer. We find that two microphases with different mobility and probably with different strength of the attachment of surfactant headgroups to the silicate surface coexist over a broad range of surfactant loadings and temperatures. An excess of surfactant with respect to the cation exchange capacity of the silicate causes plasticization of the surfactant layer in pure organoclays and appears to diminish the tendency for intercalation.

The dynamics of the surfactant layer changes already on microcomposite formation, i.e., even if no intercalation or exfoliation takes place. In such microcomposites differences in surfactant dynamics due to different surfactant loadings are diminished. For surfactant-excess organoclays, the mobility of both surfactant headgroups and tail ends decreases after composite formation, whereas for surfactant-deficient organoclays headgroup dynamics slightly speeds up. Surfactant tails and polymer molecules appear to interdigitate despite their strongly different chain lengths.

The extent of intercalation of PS into ammonium surfactant-based organoclays depends on molecular weight. The same combination of polymer and clay that leads to complete intercalation for the ammonium surfactant HTMA leads to no intercalation at all with the phosphonium surfactant HTBP.

Further elucidation of the microstructure of the surfactant layer and of its variation with surfactant loading and polymer intercalation requires additional experiments for characterizing the distribution of distances between surfactant tail ends and headgroups. A more detailed picture of interdigitation of surfactant tails and polymer chains could be obtained by applying the ESEEM experiment to a broader range of spin-labeled surfactants and polymers. Work along these lines is now in progress.

Acknowledgment. We thank Mikhail Gelfer for helpful discussions, Dariush Hinderberger for writing the program for ratio analysis of the ESEEM data, Verona Maus for performing the DSC measurements, and Christian Bauer for technical support.

Supporting Information Available: EPR spectrum of pure Somasif ME-100 and comparison of analysis of nitroxide spectra via $2A'_{zz}$ and Γ_c. This material is available free of charge via the Internet at http://pubs.acs.org.

References and Notes

(1) Blumstein, A. *J. Polym. Sci., Part A* **1965**, *3*, 2665−2672.
(2) Okada, A.; Kawasumi, M.; Usuki, A.; Kojima, Y.; Kurauchi, T.; Kamigaito, O.; In Schaefer, D. W., Mark, J. E., Eds.; *Polymer Based Molecular Composites; MRS Symp. Proc.* **1990**, *171*, 45−50.
(3) Ray, S. S.; Okamoto, M. *Prog. Polym. Sci.* **2003**, *28*, 1539−1641.
(4) Schmidt-Rohr, K.; Spiess, H. W. *Multidimensional Solid-State NMR and Polymers*; Academic Press: San Diego, 1994.
(5) Goward, G. R.; Kerr, T. A.; Power, W. A.; Nazar, L. F. *Adv. Mater.* **1998**, *10*, 449−452.
(6) Mathias, L. J.; Davis, R. D.; Jarrett, W. L. *Macromolecules* **1999**, *32*, 7958−60.
(7) VanderHart, D. L.; Asano, A.; Gilman, J. W. *Macromolecules* **2001**, *34*, 3819−22.
(8) Wong, S.; Vaia, R. A.; Giannelis, E. P.; Zax, D. B. *Solid State Ionics* **1996**, *86*−*88*, 547−557.
(9) Brik, M. E.; Titman, J. J.; Bayle, J. P.; Judeinstein, P. *J. Polym. Sci., Part B* **1996**, *34*, 2533−2542.
(10) Ishida, H., Koenig, J. L., Eds.; *Composite Interfaces*; Elsevier Science: New York, 1986.
(11) Yoon, P. J.; Hunter, D. L.; Paul, D. R. *Polymer* **2003**, *44*, 5323−5339.
(12) Chen, J.-S.; Poliks, M. D.; Ober, C. K.; Zhang, Y.; Wiesner, U.; Giannelis, E. *Polymer* **2002**, *43*, 4895−4904.
(13) Vaia, R. A.; Teukolsky, R. K.; Giannelis, E. P. *Chem. Mater.* **1993**, *5*, 1694−6.
(14) Vaia, R. A.; Giannelis, E. P. *Macromolecules* **1997**, *30*, 8000−9.
(15) Jeschke, G.; Panek, G.; Schleidt, S.; Jonas, U. *Polym. Eng. Sci.* **2004**, *44*, 1112−1121.
(16) Vaia, R. A.; Teukolsky, R. K.; Giannelis, E. P. *Chem. Mater.* **1994**, *6*, 1017−1022.
(17) Wang, L. Q.; Liu, J.; Exharos, J.; Flanigan, K. Y.; Bordia, R. *J. Phys. Chem. B* **2000**, *104*, 2810−2816.
(18) Hackett, E.; Manias, E.; Giannelis, E. P. *J. Chem. Phys.* **1998**, *108*, 7410−7415.
(19) Schweiger, A.; Jeschke, G. *Principles of Pulse Electron Paramagnetic Resonance*; Oxford University Press: Oxford, 2001.
(20) Xie, W.; Xie, R.; Pan, W.-P.; Hunter, D.; Koene, B.; Tan, L.-S.; Vaia, R. *Chem. Mater.* **2002**, *14*, 4837−4845.
(21) Hayashi, S.; Hayamizu, K. *Bull. Chem. Soc. Jpn.* **1989**, *62*, 2429−2430.
(22) Kozak, M.; Domka, L. *J. Phys. Chem. Solids* **2004**, *65*, 441−445.
(23) Bonczek, J. L.; Harris, W. G.; Nkedi-Kizza, P. *Clay Clay Mineral.* **2002**, *50*, 11−17.
(24) Maiti, P.; Yamada, K.; Okamoto, M.; Ueda, K.; Okamoto, K. *Chem. Mater.* **2004**, *14*, 4654−4661.
(25) Kurad, D.; Jeschke, G.; Marsh, D. *Biophys. J.* **2003**, *85*, 1025−1033.
(26) Gelfer, M.; Burger, C.; Fadeev, A.; Sics, I.; Chu, B.; Hsiao, B. S.; Heintz, A.; Kojo, K.; Hsu, S.-L.; Si, M.; Rafailovich, M. *Langmuir* **2004**, *20*, 3746−3758.
(27) Ichikawa, T.; Kevan, L.; Bowman, M. K.; Dikanov, S. A.; Tsvetkov, Yu. D. *J. Chem. Phys.* **1979**, *71*, 1167−1174.
(28) Tonelli, A. E. *NMR Spectroscopy and Polymer Microstructure: The Conformational Connection*; VCH: Weinheim, New York, 1989.
(29) Kurland, R. J.; McGarvey, B. R. *J. Magn. Reson.* **1970**, *2*, 286−301.
(30) Zheng, Q. H.; Yu, A. B.; Lu, G. Q.; Standish, R. K. *Chem. Mater.* **2003**, *15*, 4732−4738.
(31) Balasz, A. C.; Singh, C.; Zhulina, E. *Macromolecules* **1998**, *31*, 8370−8381.
(32) Beyer, F. L.; Tan, N. C. B.; Dasgupta, A.; Galvin, M. E. *Chem. Mater.* **2002**, *14*, 2983−2988.

MA0527449